Indian Journal of Chemistry
Vol. 57A, Aug-Sept 2018, pp. 1091-1099

Catechin mediated one-step fabrication of ZnO microspheres: Synthesis, characterization and applications

Somnath Das & Amitava Pramanik*

Unilever R&D Bangalore, 64 Main Road, Whitefield, Bangalore 560 066, India

Email: amitava.pramanik@unilever.com

Received 21 June 2018; revised and accepted 31 July 2018

A one-step template-free synthesis of hollow ZnO microspheres has been developed by a hydrothermal route in the presence of (+)-catechin as crystal habit modifier. Morphology evolution of ZnO particles shows the transformation from hexagonal rods to microspheres with increase in the concentration of catechin in the reaction medium. The microspheres are formed by the aggregation of fine grained nano-sized ZnO particles. The synthesized particles show enhanced photocatalytic ability and high potency as a drug delivery agent.

Keywords: Catechin, Zinc oxide, Microspheres, Hydrothermal, Photocatalysts

Zinc oxide (ZnO), a group II-VI semiconductor having a direct bandgap of 3.37 eV has attracted significant attention in both industry and academia, owing to its wide number of applications[1-8]. ZnO has been used extensively in photocatalysis, solar cells, optical and sensor based applications[9-15]. It is the material of choice due to its limited solubility, low toxicity, good biocompatibility and low cost. For many of its applications, the size and morphology of ZnO crystals have been tuned via crystal habit modification. Myriad shapes ranging from sphere, tetra pods, spikes, pyramids, dumbbells and flowers are amongst the common structural aggregates obtained by crystal habit modification[16-23]. The possibility of facile synthesis in the nanoscale domain, in varying shapes like zero-dimensional nanodots, one-dimensional nanorods and two-dimensional sheets that influence the bulk and surface properties of ZnO have renewed interest on this material[24-26]. However, being a semiconductor with a wide band gap at room temperature, ZnO has limited utilization of photonic energy, and thus, inferior photocatalytic efficacy compared to other materials like TiO_2.

Hierarchical structures and hollow particles are reported to boost the photo-physical and functional properties of ZnO, owing to optimal surface area, greater permeability and lower density compared to other morphologies[27-32]. Conventional processes involve templated synthesis, hydrothermal reactions and thermal evaporation techniques to synthesize such particles[33-36]. Synthesis of ZnO layers using hard templates such as carbon sphere, polystyrene beads and silica particles that can be easily eliminated from the reaction medium through dissolution or combustion is well reported in literature. In this process, both single shell and multi-shell structures have been successfully fabricated[37-40]. The other technique relies on using soft templates such as self-assemblies of macromolecules, surfactants and ionic liquids. Often, a combination of both these techniques is used for the synthesis of hollow sphere having precise control on surface and bulk properties[41, 42]. Though these methods allow control over particle size and shell thickness of hollow spherical ZnO, they are not operationally viable at a large scale, owing to multi-step processes that are cost-intensive.

In recent times, there have been attempts to use template-free routes for synthesis. The mechanism of such synthesis involves a combination of Ostwald ripening and Kirkendall-type diffusion[43-46]. Ibrahim *et al.*[47] used PVP and water/ ethanol mixture to obtain hollow spheres by maintaining a balance between the Ostwald ripening step and self-transformation. Wang *et al*. combined the cumulative effect of citrate ion induced coordination of ZnO precursor and Kirkendall effect to produce uniform hollow ZnO spheres with enhanced photocatalytic properties[48]. By suitably controlling the temperature and time of solvothermal reaction, template-free hollow

spheres were obtained by Ihara *et al.*[49] Thermal evaporation process was used for synthesis of hollow ZnO using metallic zinc at high temperature in a tube furnace[50]. Though these examples open up new approaches to achieve hollow particles, they lack the ease of synthesis, due to requirements of elevated temperature and costly experimental set-up. It was therefore pertinent to study the effect of crystal habit modifier under benign reaction conditions to obtain hollow particles.

Crystal habit modification involves small organic molecules which can selectively bind to specific crystal faces, thus regulating the crystal growth in a particular direction. Small molecules having functional groups such as carboxylates, polyhydric alcohols and amino acids are typically used in such processes. Combinations of monohydric and polyhydric alcohols have been used to produce nanoparticle-assembled hollow spherical ZnO particles by facile solvothermal route[51]. Polyol induced self-assembly of nanoparticles resulting in generation of hollow spheres has been discussed by Kim *et al.*[52] Recently, there has been emphasis on using benign polyphenolic molecules derived from extracts of common beverages like tea, coffee and wine, for modulation of ZnO morphology[53, 54]. Nanostructured ZnO particles were synthesized from extracts of both common beverages as well as some of the pure polyphenolic components viz., EGCG[55,56]. Like other commonly available flavonoids, catechin, which is abundantly present in green tea, red wine and as vegetable fluids is known to coordinate strongly with polyvalent metal ions in aqueous medium. The effect of such coordination with Zn^{2+} is also well reported in literature[57-59]. In alkaline medium, catechin and Zn^{2+} would undergo epimerization and hydrolysis respectively[60].

In the current work, we have explored the coordinating effect of (+)-catechin on ZnO crystallization in presence of a weak hydrolyzing base, as a potential template-free route to synthesize hollow microspherical particles and have explored the feasibility of using it for multifunctional benefits such as controlled delivery of a drug, ampicillin and as a superior photocatalyst.

Materials and Methods

All chemicals were of analytical grade and used without further purification. Zinc nitrate hexahydrate ($Zn(NO_3)_2.6H_2O$, AR grade), hexamethylenetetramine (HMTA, $C_6H_{12}N_4$, AR grade) and (+)-catechin hydrate ($C_{15}H_{14}O_6$, AR grade) were procured from Sigma-Aldrich. Distilled water used in all experimental processes had the following characteristics: pH 7.2–7.4, electrical conductance 2×10^{-6} S cm^{-1}, total dissolved salt < 0.5 mg/L and turbidity <0.1 NTU.

Synthesis of ZnO particles

ZnO particles were synthesized by following a conventional hydrothermal route using $Zn(NO_3)_2.6H_2O$ as the source of zinc ions and HMTA as slow hydrolyzing base at elevated temperature. Briefly, 50 mM of $Zn(NO_3)_2.6H_2O$ (1.49 g, 0.1 M) and 50 mM of HMTA (0.70 g, 0.1 M) were mixed at room temperature in sealed autoclave containers, stoppered and heated in an air oven for 3 h. For reactions where (+)-catechin was used as additive to affect crystal habit, requisite amount of additive was completely dissolved in the $Zn(NO_3)_2.6H_2O$ stock solution to obtain a clear solution. This solution was mixed with HMTA and the reaction was carried out for 3 h. On completion of the reaction, the reaction mixtures were cooled to room temperature and the particles were filtered through Whatman 40 filter paper. The precipitate was washed thoroughly with deionized water followed by copious amounts of ethanol and dried in air. For studying the kinetics of formation of ZnO, the reaction was quenched at different intervals of time and the particles formed were analyzed. The compositions of the different sets of reaction are given in Table 1.

Characterization

Powder X-ray diffraction (PXRD) pattern of the synthesized ZnO particles were taken using a Rigaku Ultima IV diffractometer using Cu-Kα (λ = 1.5406 Å) radiation with a step size of 0.1°/s and 2θ angle between 20° to 70°. Joint committee for powder diffraction standards (JCPDS, card number 36-1451) was used to assign XRD peak positions and relative intensities. Scanning electron microscope (SEM) was used to ascertain the morphological evolutions of the synthesized particles using a Hitachi S-4700 machine at an accelerating voltage of 10 kV. Energy

Table 1 — Compositions of reactant and habit modifier for synthesis of ZnO particles

Sample	$Zn(NO_3)_2.6H_2O$ (mM)	HMTA (mM)	Additive (mM)	Mole ratio (additive:zinc)
ZnO-1	50	50	0.0	-
ZnO-2	50	50	0.5	1:100
ZnO-3	50	50	1.0	1:50
ZnO-4	50	50	10	1:5

dispersive X ray analysis (EDXA) was used to determine the elemental composition of the particles. High resolution transmission electron microscopy (HRTEM) was performed using JEOL-TEM 2100 microscope with an operating voltage of 200 kV to image the crystallite shape and the lattice fringes. Room temperature Fourier transform infrared (FTIR) measurements were made on a Perkin-Elmer FTIR spectrophotometer (model Spectrum-1) with a resolution of 4 cm^{-1} using the KBr pellet technique. Pyris thermal analyzer (model Pyris-1 TGA) was used to determine decomposition components under a dry N_2 flow from 25 °C to 700 °C at a heating rate of 10 °C min^{-1}. Calcination of the ZnO samples was done at 400 °C, 500 °C and 600 °C using a muffle furnace. The BET surface area was calculated using a BET surface analyzer (Smart Instruments) for the synthesized ZnO samples and average pore sizes were calculated.

Photocatalytic activity

Photocatalytic efficacy of the calcined ZnO powders was studied by following the degradation of methylene blue dye. The synthesized ZnO (5 mg) was added to 100 mL of 20 μM dye solution taken in a photocatalytic reactor. The suspension was then irradiated with UV light from a mercury lamp (60 W, 365 nm) under constant stirring condition (400 rpm, 25 °C). Aliquots were taken out from the reactor at every 5 minutes during irradiation, centrifuged and their absorbance were recorded at 664 nm (absorbance maxima of methylene blue in water) using a Perkin-Elmer Lambda-35 UV-vis spectrophotometer. Blank dye degradation was also carried out under similar condition without adding the catalyst.

The drug delivery of ampicillin antibiotic was studied by loading the drug on different ZnO particles. Ampicillin sodium salt (0.5 g) was dissolved in 100 mL deionized water. To this solution (25 mL), ZnO particles (50 mg) were added. The mixture was stirred using a magnetic stirrer for 2 h. The drug loaded particles were centrifuged at 5000 rpm for 5 min and washed thoroughly with distilled water 3 times. The resultant particles were dried under vacuum overnight. The drug loading on the particles was examined by TGA analysis prior to the drug release profile evaluation. To study the drug release profile, 50 mg of the drug loaded ZnO particles, were suspended in 50 mL of PBS buffer and agitated in a reciprocating shaker at 200 rpm. Aliquots were drawn out from the supernatant solution at specific intervals of time and passed through a 0.45 μm syringe filter. For every aliquot withdrawal, 3 mL of fresh PBS buffer was replenished in the solution to maintain constant volume. Spectrophotometric quantification of the drug released in solution was measured at 268 nm corresponding to the λ_{max} of ampicillin molecule.

Results and Discussion

Synthesis of ZnO particles

Synthesis of ZnO by hydrothermal route was carried out at 95 °C using zinc nitrate and hexamethylenetetramine (HMTA) as reactants. Typical reaction for the formation of ZnO proceeds through the following reaction sequences[61]:

$$C_6H_{12}N_4 + 10H_2O \rightarrow 6HCHO + 4NH_4OH \quad \ldots (1)$$

$$Zn(NO_3)_2 \rightarrow Zn^{2+} + 2NO_3^- \quad \ldots (2)$$

$$NH_4OH \rightarrow NH_4^+ + OH^- \quad \ldots (3)$$

$$Zn^{2+} + 2OH^- \rightarrow ZnO + H_2O \quad \ldots (4)$$

The reaction involves generation of ammonia at an elevated temperature due to hydrolysis of HMTA in the first step. The second step involves the reaction of zinc salt with the alkaline ammonia solution to produce crystalline ZnO particles. It is well studied in literature that presence of ligands which easily associate with Zn^{2+} ions can lead to morphological diversities in the precipitated ZnO crystal due to their influence on the kinetics of crystallization and relative binding onto specific crystal planes[62]. Metal complexation with polyphenols such as quercetin, rutin and catechin has been extensively studied[59, 63-65]. Zinc is the first transition series element having 10 *d* electrons in its outermost shell, which lowers its ability to form a complex compared to other counterparts. However, it is still known to bind preferentially with hydroxyl groups in polyphenolic compounds resulting in the formation of stable zinc-polyphenol complexes[53-55]. (+)-Catechin being highly water soluble and one of the abundant natural polyphenol was chosen as a suitable modifier owing to its ability to bind with Zn^{2+} in aqueous medium, which in turn could affect the kinetics of nucleation and crystal growth of the ZnO particles. In the present study, extent of crystal habit modification was varied by adding various concentrations of (+)-catechin in the reaction medium in the beginning of the reaction.

Morphology of ZnO: SEM and TEM studies

It is evident from Fig. 1, that in the absence of any modifier, hexagonal rod-like ZnO particles with

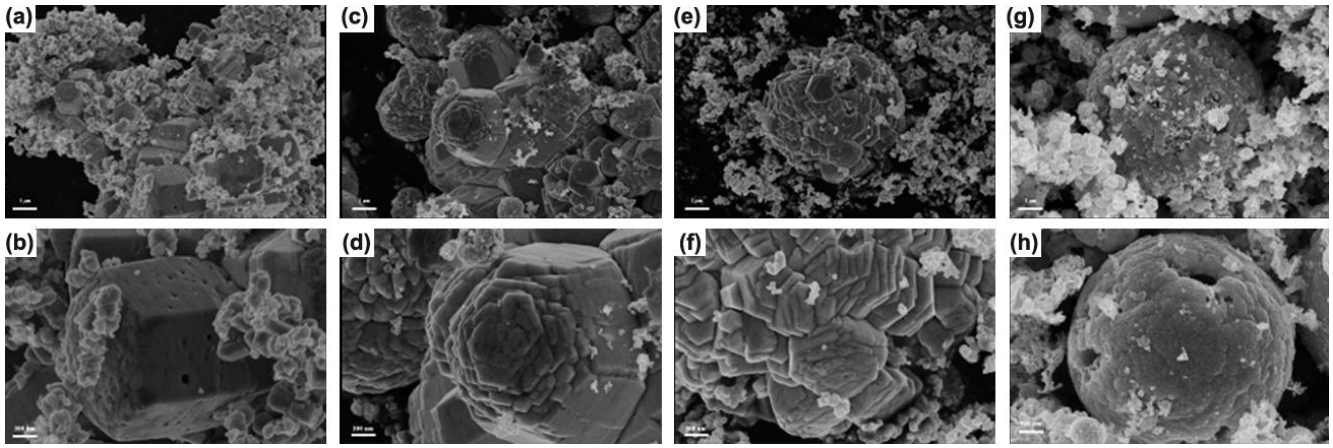

Fig. 1 — SEM images of ZnO particles synthesized in presence of varying amounts of (+)-catechin. [(a, b) 0; (c, d) 0.5; (e, f) 1.0; (g, h) 10 mM. [b, d, f, h are higher resolution SEM images of a, c, e, g respectively].

varied particle sizes were formed. However, in the presence of (+)-catechin, morphological diversities were observed and extent of variation increased with increase in the concentration of catechin in the reaction medium. At very low concentration of catechin (0.5 mM), tapering in the hexagonal rod morphology was observed which became more pronounced with increase in the concentration of modifier.

Catechin is a polyphenol and thus presents possibilities of complexing with the Zn^{2+} ion through coordinate bonding where oxygen atom acts as the electron donor. It can be hypothesized that this interaction facilitates the prolongation of the nucleation step (reaction 4) in the formation of ZnO which in turn regulates the crystal growth[17]. Additionally, the catechin moiety is expected to have greater affinity to the (0001) plane of the ZnO crystal owing to the polar nature of the crystal and the relative abundance of Zn^{2+} ions in the lattice positions in this plane[17]. Such kind of binding may affect the final morphology of ZnO particles by making them more suppressed along the *c* axis. As is evident from our study, increase in the catechin content transformed the free forming hexagonal rod morphology to clusters of hexagonal disks eventually forming microspherical structures. It is worth mentioning that the microspherical structures formed in the presence of a significantly large concentration of catechin (10 mM) was found to have small openings and that it is formed by the aggregation of large number of fine grained ZnO nanoparticles.

Pure and crystalline wurtzite ZnO phase with distinct lattice fringes having a *d* spacing of 0.26 nm corresponding to (002) crystal plane could be identified on the surface of the ZnO microspheres from TEM measurements (Fig. 2). The surface of the ZnO microspheres appear to be interspaced with a combination of nanocrystalline ZnO and a non-descriptive phase, which may result due to the adsorbed catechin in the ZnO matrix or the subsequent complexation with Zn^{2+} ions. This leads us to the conjecture that the ZnO microspheres are formed by the aggregation of nanoparticulate ZnO with primary crystallite size of ~2.5–5 nm. This is further confirmed by the SEM study where we have visualized the ZnO microspheres formed by aggregation of ZnO nanocrystals. This assemblage is evidently influenced by a large amount of catechin in the reaction medium, which complexes extensively with the Zn^{2+} ions, thus subduing its rate of conversion to ZnO. Also, the catechin adsorbed on the surface of ZnO crystals may also regulate the evolution of this unique structure possibly by facilitating 'cohesive fusion' of the crystals at the initial stage of the reaction as shown in Fig. 3.

Growth kinetics of the microspherical ZnO particles was studied by withdrawing small portions of the reaction volume and analyzing the nature of the particles formed at different intervals of time. The study was done for ZnO-4 sample, since it resulted in microspheres. It is evident from Fig. 4 that morphology evolution of ZnO proceeds through the formation of non-descriptive agglomeration of particles at the start of the reaction followed by the formation of nanospheres which eventually fuse and grow to larger microspherical assemblages. With increase in time of the reaction, the transformation of

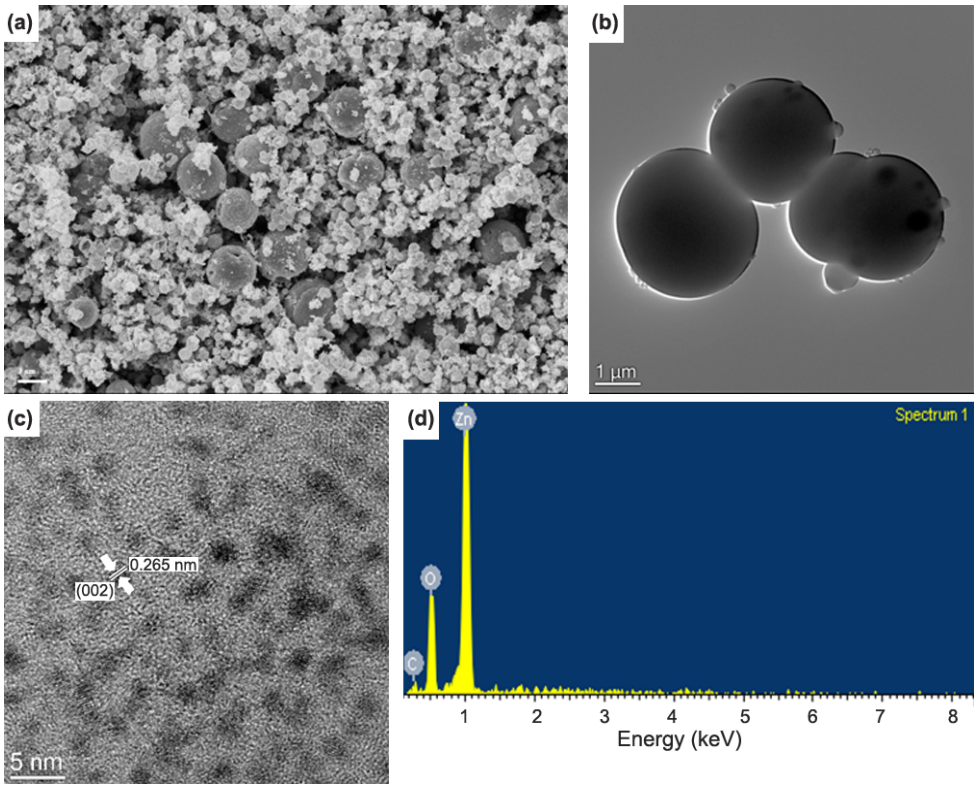

Fig. 2 — (a) SEM, (b) TEM, (c) HRTEM images of ZnO-4 microspheres showing (002) plane of wurtzite ZnO. (d) EDX spectrum.

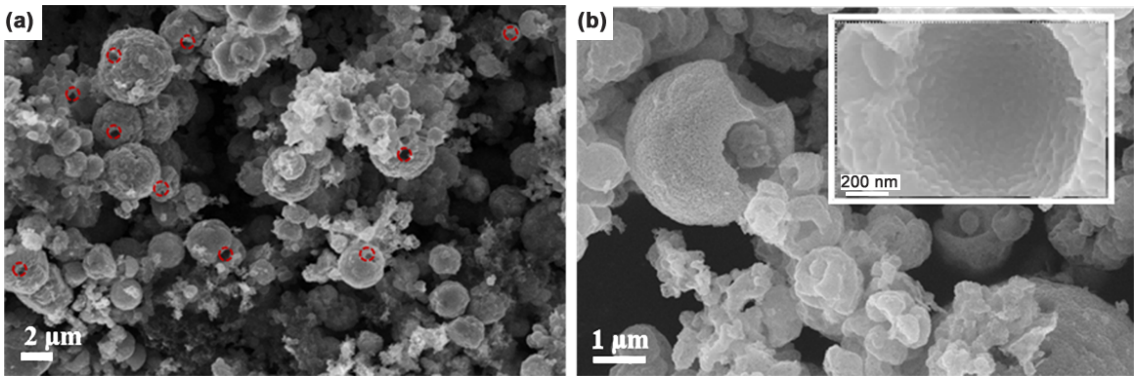

Fig. 3 — FESEM images of ZnO-4 microspheres synthesized in bulk at different magnifications. [Red circles in (a) indicate the holes on the spherical surface].

nanostructure to micro-structured spheres with adequate surface roughness was observed, which may be indicative of the adsorption of the carbon rich catechin moiety onto ZnO particles.

The presence of high quantity of carbon arising from the catechin moiety in the matrix of spherical ZnO particles was further evidenced by EDX mapping (Supplementary Data, Fig S1). Subsequently, the synthesized spherical ZnO was calcined to remove the organic content. Post calcinations, the EDX spectra showed significant reduction in the carbon content in the calcined ZnO samples.

Characterization

X-ray crystallography of the samples were performed to elucidate the crystallinity of the material synthesized in the presence of (+)-catechin as crystal habit modifier. The comparative XRD plot of different samples is shown in Fig. 5. All samples showed the characteristic peaks of wurtzite form of ZnO (JCPDS no. 36-1451) and no peaks corresponding to intermediate compounds were observed. This clearly shows that pure phase ZnO with varied morphologies could be synthesized in the presence of catechin as modifier, and transient

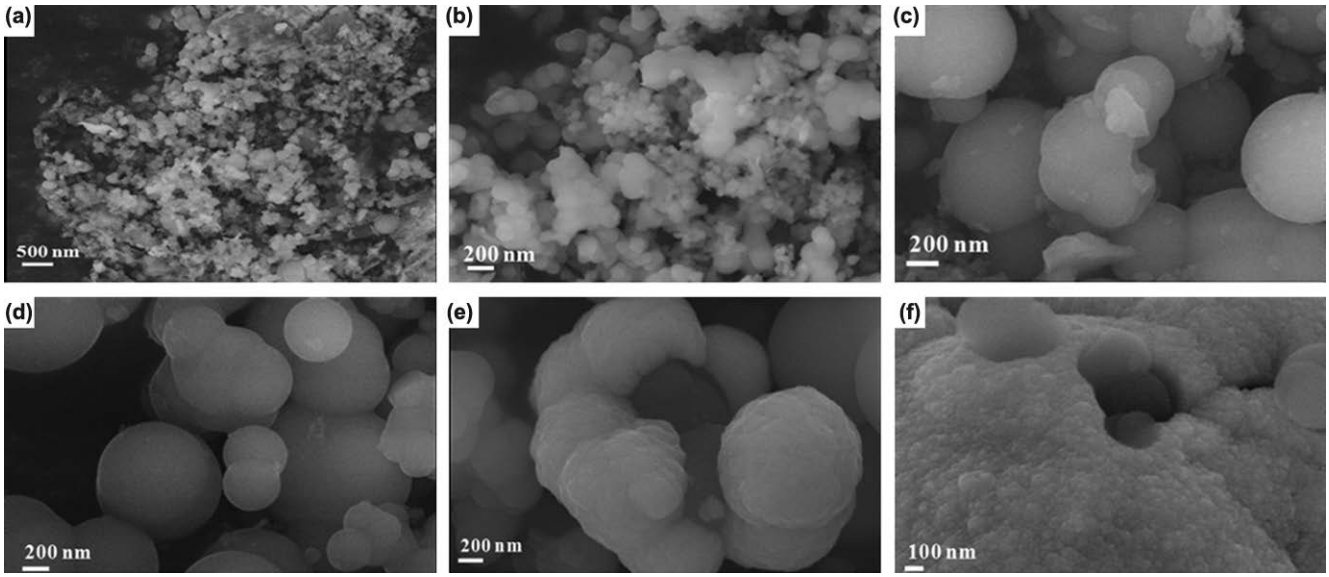

Fig. 4 — FESEM images depicting the growth kinetics of ZnO-4 microspheres after (a) 10, (b) 20, (c) 30, (d) 45, (e) 60, and, (f) 90 min of reaction.

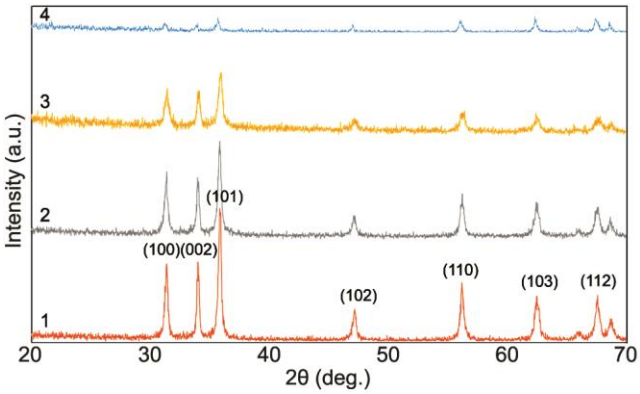

Fig. 5 — XRD profiles of synthesized ZnO particles. [(1) ZnO-1; (2) ZnO-2; (3) ZnO-3; (4) ZnO-4].

complexation which may arise at the intermediate stage of the reaction does not remain in the ZnO matrix at the completion of the reaction. We also observed a consequent decrease in the X-ray diffraction intensity as the concentration of catechin increased in the reaction mixture, which essentially shows that substantial part of the catechin remains trapped in the ZnO matrix and that crystallization is possibly affected by the presence of catechin, thus promoting more amorphous type particles.

To further investigate the presence of entrapped catechin in the ZnO particles, FTIR analysis of the synthesized samples were done. The comparative plot of catechin alone vis-à-vis ZnO particles synthesized in presence of catechin is presented in Fig. S2 (Supplementary Data). It is evident from the FTIR spectra that prominent catechin peaks are observed in the spectra of the synthesized particles and the peak intensity increases with increase in the concentration of catechin in the ZnO matrix. The characteristic peaks corresponding to C-H alkenes (970 cm^{-1}), C-O (1030 cm^{-1}, 1280 cm^{-1}), aromatic O-H (1143 cm^{-1}), C-H alkanes (1470 cm^{-1}) and aromatic C=C stretching (1519 cm^{-1}) were detected in pure catechin sample and signature peaks were also found in the ZnO composite particles synthesized in presence of catechin. Further, we observed significant shift in the peak at 1519 cm^{-1} and 1612 cm^{-1} to 1497 cm^{-1} and 1607 cm^{-1} respectively in the ZnO samples. Also, the absence of 1030, 1143 and 1470 cm^{-1} peaks in the ZnO samples were suggestive of possible chemical association of the catechin molecule to Zn^{2+} in addition to being adsorbed onto the surface.

To corroborate the FTIR results, thermogravimetric analysis of the samples synthesized in presence of varying concentrations of catechin was performed. It is evident from Fig S3 (Supplementary Data), that incorporation of substantial amount of organic matter in the ZnO matrix takes place. Pure catechin undergoes several weight losses between 100 °C and 350 °C corresponding to the loss of -OH groups 175–177 °C and consequent decomposition at higher temperatures. The characteristic decomposition weight losses between 275–350 °C were found in the synthesized ZnO samples, ascertaining that catechin is associated in the crystal matrix. The extent of catechin present in the ZnO matrix increased with the increase in concentration of catechin used during the synthesis.

Photocatalytic efficacy

Photocatalytic studies were performed on calcined ZnO samples prepared by annealing the as-prepared samples at varied temperatures, in order to remove the adsorbed catechin and check the efficacy on the resultant calcined materials. The degradation of an anionic dye, methylene blue (MB) was monitored using calcined ZnO particles under UV light irradiation. For the study, ZnO-4 samples were calcined separately at 400 °C, 500 °C and 600 °C respectively and compared with calcined (600 °C) conventional hexagonal ZnO rods (ZnO-1) as shown in Fig. 6. MB dye is known to undergo degradation in the presence of UV light, which is enhanced considerably by the presence of ZnO catalyst. In the presence of ZnO-4, photodegradation of dye for all samples followed pseudo-first order kinetics with the rate of degradation in the following order: $ZnO_{cal600°} > ZnO_{cal500°} > ZnO_{cal400°} > ZnO_{conventional} >$ MB. The calculated rate constants for dye degradation of the above samples were 0.0842, 0.0728, 0.0439, 0.0399 and 0.017 min^{-1} respectively. The enhancement in the photocatalytic efficacy with increase in the calcination temperature may be attributed to the superior photosensitization of dye molecule by the ZnO particle as the calcination temperature is increased. It can be envisaged that higher calcination temperature aids in modulating ZnO microstructures by effectively removing the organic modifier. Also, with increase in calcination temperature there is a consequent increase in the crystallite size. Mechanistic interpretation of photocatalysis suggests that the generation of OH radicals during photooxidation process drives photo catalysis. We estimated the OH index of the materials to correlate with their photocatalytic efficiency. For this purpose, P25 titanium dioxide (obtained from Degussa) is taken as benchmark (indexed as 100) for calculating the OH index of other materials (Supplementary Data, Fig S4). The OH index of commercially available ZnO is reported in literature to be 16.4. In comparison, the OH index determined for calcined ZnO-4 at 600 ºC was found to be 86.8, thus showing significant improvement in the efficiency of photocatalysis by ZnO particles, which has been achieved by suitably controlling the crystal growth and the calcination temperature. No morphological changes of the ZnO particles were observed upon photocatalytic degradation of the dye on its surface.

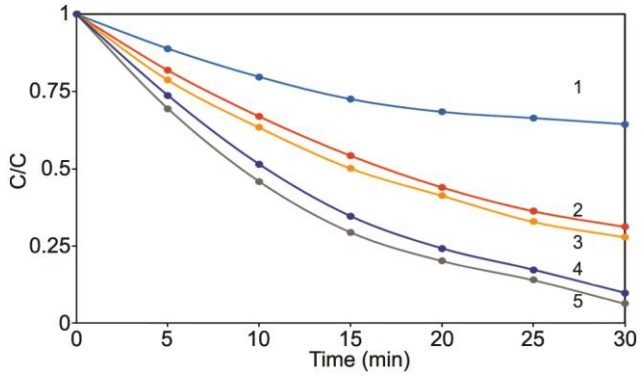

Fig. 6 — Photocatalytic degradation profile of MB dye. [(1) No ZnO; (2) ZnO-1 calcined at 600 °C; ZnO-4 calcined at (3) 400 °C, (4) at 500 °C, and, (5) at 600 °C].

Efficacy of drug delivery

To evaluate the potency of using the synthesized microspherical ZnO as a delivery vehicle for drugs, a study was done on a model drug, ampicillin. Ampicillin belongs to the group of beta-lactam antibiotics and is commonly used as a broad-spectrum antibiotic that can be administered therapeutically to control both gram-positive and gram-negative bacterial infections[69]. Ampicillin is (2S,5R,6R)-6-([(2R)-2-amino-2-phenylacetyl]amino)-3,3-dimethyl-7-oxo-4-thia-1-azabicyclo [3.2.0]heptane-2-carboxylic acid having the formula $C_{16}H_{19}N_3O_4S$. In recent times, several attempts have been made to develop efficient drug delivery agents, selected from both inorganic carriers and organic encapsulates to affect the delivery efficacy, sustained release and targeted dispensation of the drug molecules. Amongst the inorganic carriers, often insoluble benign particles selected from ZnO, $CaCO_3$ and TiO_2 have been used[70, 71]. ZnO has been extensively analyzed by the Food and Drug Administration in the United States and classified as a safe ingredient for therapeutic use[72]. It was also demonstrated that by increasing the surface-to-volume ratio of these compounds it is possible to improve the drug loading and sustained release profile of the composites. For this purpose, concerted efforts were undertaken to synthesize shape selective nanoparticles for optimal performance. Courrier *et al.*[73] demonstrated that particle size of less than 50 nm is preferred since it can penetrate the cell barrier and thus deliver the drug at the source. However, being nanoparticles, they pose a serious threat of being cytotoxic if the dosage is not controlled appropriately. The challenge therefore lies in delivering the sustained release profile of the drug from a microparticulate composite. It is well reported in literature that the microstructure

of the carrier and the nature of interaction between the drug molecule play a critical role on the drug delivery efficacy[74]. Ampicillin has three distinct UV absorption peaks at 257, 262 and 268 nm respectively. In this study, we have investigated the adsorption and subsequent release profile of ampicillin drug molecule on the morphologically derived ZnO particles by spectrophotometric technique by monitoring the change in peak intensity at 268 nm. The experiment was performed in two stages. At first, ampicillin was loaded on ZnO-1 and ZnO-4 particles respectively, under identical conditions to distinguish the effect of morphological and microstructural changes for rod-like and hollow-spherical particles on the drug loading. Conditions were optimized according to the described method to ascertain similar level of drug loading on both the particles. The loading for ZnO-1 and ZnO-4 were 6.3% and 5.9% by weight respectively obtained by the thermogravimetric analysis. (Supplementary Data, Fig S5). The drug release profiles of ZnO-1 and ZnO-4 are presented in Fig. S6 (Supplementary Data). It is evident from the data that drug release is consistent as the time progresses from 1 h to 24 h for both ZnO-1 and ZnO-4. The release profile shows greater delivery in the initial time scale which progressively becomes saturated with time. It is interesting to note that the release profile is higher for ZnO-1 compared to ZnO-4 for similar loading of the drug. The ratio of drug release of ZnO-1: ZnO-4 was 2.5, 1.5, 1.2 and 1.1 times corresponding to 1, 2, 3 and 4 h respectively. The release of drug tends to saturate with increase in time and with 24 h exposure, the microstructural effect was not found to be significant. The result evidently shows that ZnO-4 can retain the drug molecule more compared to ZnO-1 and thus act as a better agent for sustained release of ampicillin drug. This observation can be explained on the basis of the relative size and surface area difference between ZnO-1 rods and ZnO-4 microspheres. It is known that with a decrease in size of particle, there is a consequent increase in the surface area to volume ratio. Wim *et al.*[74] demonstrated that lowering the surface area for a given size, results in lowering of the leaching rate of the drug from the core of the microspheres compared to that of the rods. Additionally, the physical entrapment of drug molecules in the hollow spaces may aid in their sustained release profile.

Conclusions

In this work, we have demonstrated a one-step hydrothermal route to synthesize ZnO hollow microspheres using (+)-catechin as crystal habit modifier. The concentration of the crystal habit modifier played a critical role in tuning the morphology from rod-like to spherical shape, with small openings on the surface. The microspheres were formed by the aggregation of nanoparticulate ZnO. The synthesized microspherical particles showed improved photocatalytic and drug delivery properties which can be compared to conventional counterparts.

Supplementary Data

Supplementary data associated with this article are available in the electronic form at http://www.niscair.res.in/jinfo/ijca/IJCA_57A(8-9)1091-1099_SupplData.pdf.

Acknowledgement

The authors would like to thank Centre For Nano-Science and Engineering (CeNSE), Indian Institute of Science, Bangalore, India, for the FESEM images. Indian Association for the Cultivation of Science, Kolkata, India, is gratefully acknowledged for the TEM analysis.

References

1 Srikant V & Clarke D R, *J Appl Phys*, 83 (1998) 5447.
2 Zhang Y, Nayak T R, Hong H & Cai W, *Curr Mol Med*, 13 (2013) 1633.
3 Moezzi A, McDonagh A M & Cortie M B, *Chem Eng J*, 185/186 (2012) 1.
4 Klingshirn C, *ChemPhysChem*, 8 (2007) 782.
5 Baruah S & Dutta J, *Sci Technol Adv Mater*, 10 (2009) 013001.
6 Zhang Y, Ram M K, Stefanakos E K & Goswami D Y, *J Nanomater*, 2012 (2012) 624520.
7 Weintraub B, Zhou Z, Li Y & Deng Y, *Nanoscale*, 2 (2010) 1573.
8 Wang Z L, *Chin Sci Bull*, 54 (2009) 4021.
9 Height M J, Pratsinis S E, Mekasuwandumrong O & Praserthdam P, *Appl Cat B: Environ*, 63 (2006) 305.
10 Sharma A, Rao P, Mathur R P & Ameta S C, *J Photochem Photobiol A: Chem*, 86 (1995) 197.
11 Poulios I & Tsachpinis I, *J Chem Technol Biotechnol*, 74 (1999) 349.
12 Chou T P, Zhang Q, Fryxell G E & Cao G, *Adv Mater*, 19 (2007) 2588.
13 Ko S H, Lee D, Kang H W, Nam K H, Yeo J Y, Hong S J, Grigoropoulos C P & Sung H J, *Nano Lett*, 11 (2011) 666.
14 Zhang Q, Dandeneau C S, Zhou X & Cao G, *Adv Mater*, 21 (2009) 1.
15 Dutta K, Das S & Pramanik A, *J Colloid Interf Sci*, 366 (2012) 28.

16 Pan H, Misra N, Ko S H, Grigoropoulos C P, Miller N, Haller E E & Dubon O, *Appl Phys A*, 94 (2009) 111.
17 Das S, Dutta K & Pramanik A, *CrystEngComm*, 15 (2013) 6349.
18 Garcia S P & Semancik S, *Chem Mater*, 19 (2007) 4016.
19 Das S & Ghosh S, *Dalton Trans*, 42 (2013), 1645.
20 Mclaren A, Valdes-Solis T, Li G & Tsang S C, *J Am Chem Soc*, 131 (2009) 12540.
21 Yang L Y, Dong S Y, Sun J H, Feng J L, Wu Q H & Sun S P, *J Hazardous Mater*, 179 (2010) 438.
22 Li P, Wei Z, Wu T, Peng Q & Li Y, *J Am Chem Soc*, 133 (2011) 5660.
23 Chen Z G, Ni A, Li F, Cong H, Cheng H M & Lu G Q, *Chem Phys Lett*, 434 (2007) 301.
24 Das S, Meena S S & Pramanik A, *J Colloid Interf Sci*, 462 (2016) 307.
25 Weintraub B, Zhou Z, Li Y & Deng Y, *Nanoscale*, 2 (2010) 1573.
26 Xiong D, Fang T, Yu L, Sima X & Zhu W, *Sci Total Environ*, 409 (2011) 1444.
27 Barman M K, Mitra P, Bera R, Das S, Pramanik A & Patra A, *Nanoscale*, 9 (2017) 6791.
28 Mitra P, Barman M K, Basu S, Das S, Pramanik A & Patra A, *ChemistrySelect*, 2 (2017) 9869.
29 Zhu Z, Yang D & Li H, *Adv Powder Tech*, 22 (2011) 493.
30 Lan S, Liu L, Li R, Leng Z & Gan S, *Ind Eng Chem Res*, 53 (2014) 3131.
31 Lu F, Cai W & Zhang Y, *Adv Funct Mater*, 18 (2008) 1047.
32 Mousavi S M, Mahjoub A R & Abazari R, *RSC Adv*, 5 (2015) 107378.
33 Caruso F, Caruso R A & Möhwald H, *Science*, 282 (1998) 1111.
34 Obare S O, Jana N R & Murphy C J, *Nano Lett*, 1 (2001) 601.
35 Lallave M, Bedia J, Ruiz-Rosas R, Rodríguez-Mirasol J, Cordero T, Otero J C, Marquez M, Barrero A & Loscertales I G, *Adv Mater*, 19 (2007) 4292.
36 Tringe1 J W, Levie1 H W, El-Dasher B S, Swift R & Wall M A, *Appl Phys Lett*, 98 (2011) 241907.
37 Jia X, Fan H, Zhang F & Qin L, *Ultrason Sonochem*, 17 (2010) 284.
38 Wang X, Hu P, Fangli Y & Yu L, *J Phys Chem C*, 111 (2007) 6706.
39 Zeng X, Yang J, Shi L, Li L & Gao M, *Nanoscale Res Lett*, 9 (2014) 468.
40 Wang X, Liao M, Zhong Y, Zheng J Y, Tian W, Zhai T, Zhi C, Ma Y, Yao J, Bando Y & Golberg D, *Adv Mater*, 24 (2012) 3421.
41 Wang X, Hu P, Fangli Y & Yu L, *J Phys Chem C*, 111 (2007) 6706.
42 Jia X, Fan H, Zhang F & Qin L, *Ultrason Sonochem*, 17 (2010) 284.
43 Xu H L, Wang W Z, Zhu W & Zhou L, *Nanotech*, 17 (2006) 3649.
44 Cao X B, Gu X, Zhuge L, Gao W J, Wang W C & Wu S F, *Adv Funct Mater*, 16 (2006) 896.
45 Yin Y D, Rioux R M, Erdonmez C K, Hughes S, Somorjai G A & Alivisatos A P, *Science*, 304 (2004) 711.
46 Lin G, Zheng J & Xu R, *J Phys Chem C*, 112 (2008) 7363.
47 Ibrahim A M, Abd El-Latif M M & Gohr M S, *Egypt J Chem*, 58 (2015) 475.
48 Wang M, Cao X, Wang L & Zhang L, *J Porous Mater*, 17 (2010) 79.
49 Iharaa T, Wagatab H, Kogurec T, Katsumataa K, Okadaa K & Matsushita N, *RSC Adv*, 4 (2014) 25148.
50 Cheng J, Yang X, Tian H, Zhao B & Zhang D, *Adv Mater Sci Eng*, (2014) ID: 567278.
51 Jiang J, Zhang K, Chen X, Zhao F, Xie T, Wang D & Lin Y, *J Alloys Comp*, 699 (2017) 907.
52 Kim S W, Nguyen T K, Thuan D V, Dang D K, Hur S H, E, Kim E J & Hahn S H, *Korean J Chem Eng*, 34 (2017) 495.
53 Vayssieres L, Keis K, Lindquist S E & Hagfeldt A, *J Phys Chem B*, 17 (2001) 3350.
54 Mclaren A, Valdes-Solis T, Li G & Tsang S C, *J Am Chem Soc*, 131 (2009) 12540.
55 Sutradhar P, Debbarma M & Saha M, *Synth React Inorg, Metal-Org Nano-Metal Chem*, 46 (2016) 1622.
56 Suresh D U, Nethravathi P C, Lingaraju K, Rajanaika H, Sharma S C & Nagabhushana H, *Spectrochim Acta, Part A: Mol Biomol Spect*, 136 (2015) 1467.
57 Wang X W, Jiang G & Du J G, *Acta Phys Chim Sin*, 27 (2011) 309.
58 Esparza I, Salinas I, Santamar´ıa C, Garc´ıa-Mina J M & Fern´andez J M, *Anal Chim Acta*, 543 (2005) 267.
59 Bark K M, Yeom J E, Yang I J, Park O H, Park C H & Park H R, *Bull Korean Chem Soc*, 33 (2012) 12.
60 Ishino N, Yanase E & Nakatsuka S I, *Biosci Biotechnol Biochem*, 74 (2010) 875.
61 Ladanov M, Ram M K, Matthews G & Kumar A, *Langmuir*, 27 (2011) 9012.
62 Agnieszka K R & Teofil J, *Materials (Basel)*, 7 (2014) 2833.
63 de Souza R F V & de Giovani W F, *Spectrochim Acta Part A: Mol Biomol Spect*, 61 (2005) 1985.
64 de Souza R F V & de Giovani W F, *Redox Report*, 9 (2004) 97.
65 Tan J, Wang B & Zhu L, *Bioorg Med Chem*, 17 (2009) 614.
66 Nest G L, Caille O, Woudstra M, Roche S, Burlat B, Belle V, Guigliarelli B & Lexa D, *Inorg Chim Acta*, 357 (2004) 2027.
67 Yasarawan N, Thipyapong K, Sirichai S & Ruangpornvisuti V, *J Mol Struct*, 1047 (2013) 344.
68 Bodini M E, del Valle M A, Tapia R, Leighton F & Berrios P, *Polyhedron*, 20 (2001) 1005.
69 Carafa M, Marianecci C, Lucania G, Marchei E & Santucci E, *J Contr Rel*, 95 (2004) 67.
70 Palanikumar L, Ramasamy S, Hariharan G & Balachandran C, *Appl Nanosci*, 3 (2013) 441.
71 Aw M S & Losic D, *Int J Pharm*, 443 (2013) 154.
72 https://www.accessdata.fda.gov/scripts/cdrh/cfdocs/cfcfr/CFRSearch.cfm?fr=182.8991, Cite: (21CFR182.8991)
73 Courrier H M, Butz N & Vandamme T F, *Crit Rev Ther Drug Carrier Syst*, 19 (2002) 425.
74 Jong W H D & Borm P J A, *Int J Nanomed*, 3 (2008) 133.